RESEARCH ARTICLE

Key Points:
- The NEC bifurcation is modulated by Rossby waves to the east
- Rossby wave generation is closely related to wind stress curl pattern
- It is not proper to consider wind field in the same frame for all years

Correspondence to:
C.-R. Wu,
cwu@ntnu.edu.tw

Modulation of Rossby waves on the Pacific North Equatorial Current bifurcation associated with the 1976 climate regime shift

Li-Chiao Wang[1], Chau-Ron Wu[1], and Bo Qiu[2]

[1]Department of Earth Sciences, National Taiwan Normal University, Taipei, Taiwan, [2]Department of Oceanography, University of Hawaii at Manoa, Honolulu, Hawaii, USA

Abstract Simulated current velocity and long-term reanalysis wind data are used to investigate interannual variations in the bifurcation of the Pacific North Equatorial Current (NEC) after the 1976 climate regime shift. Wind stress curl anomaly (WSCA) in the region of $10°N–15°N$ and $160°E–170°E$ generates Rossby waves and affects the NEC bifurcation along the Philippine coast. From 1976 to 1992, following a regime shift to the positive Pacific Decadal Oscillation (PDO) phase, PDO and El Niño-Southern Oscillation (ENSO) match each other in strength and have a neutralized effect on the WSCA. From 1993 to 2009, WSCA matches PDO well, and its correlation with ENSO is lower. Using a linear regression model, we show that the influence of PDO has nearly 13 times weight over that of ENSO. Prior to the 1976 regime shift, WSCA is closely related to ENSO from 1961 to 1975, and it does not correlate significantly with PDO. Our analysis results show that Rossby waves are preferentially generated in either the negative PDO phase when the ENSO signal dominates, or in the positive PDO phase when the ENSO signal is overshadowed. In the phase when the positive PDO counteracts with the ENSO signal, neither ENSO nor PDO has a significant influence on Rossby wave generations through the WSCA.

1. Introduction

In the western North Pacific Ocean, the westward flowing North Equatorial Current (NEC) splits as it encounters the Philippine coast. The poleward-flowing branch forms the root of the Kuroshio, while the equatorward-flowing branch becomes the Mindanao Current (MC). Both of these western boundary currents ultimately recirculate eastward as the Kuroshio Extension and the North Equatorial Countercurrent (NECC), indicating that the NEC plays a noticeable role in regulating the North Pacific subtropical and tropical gyres. Specifically, the bifurcated NEC provides important pathways for heat, mass, and salt transport exchanges between the Kuroshio and MC, which approximately represent the midlatitude and low-latitude western North Pacific, respectively [*Lukas et al.*, 1991]. Therefore, variation in the NEC bifurcation latitude, accompanied by a quantitative change in the partitioning of the NEC transport between the Kuroshio and MC [e.g., *Qiu and Lukas*, 1996; *Kim et al.*, 2004], plays an essential role in midlatitude and low-latitude circulation changes.

Seasonal variation in the NEC bifurcation has been frequently debated and discussed. *Qu and Lukas* [2003] used hydrographic data to show that the bifurcation latitude occurs at its southernmost position in July and at its northernmost position in December. Several studies based on model outputs and satellite altimeter measurements revealed a similar seasonality [e.g., *Kim et al.*, 2004; *Qiu and Chen*, 2010]. Separately, using a reduced-gravity ocean model, *Qiu and Lukas* [1996] estimated the NEC bifurcation to be at its southernmost latitude in April/May and its northernmost latitude in October/November (*Qui and Lukas*, 1996, Figure 9). Furthermore, the NEC bifurcation latitude is thought to be related to the wind forcing, consisting of the local monsoon and remote forcing by Rossby waves [*Qiu and Lukas*, 1996]. During the northeast monsoon, positive wind stress curl (WSC) forms an anomalous cyclonic circulation around the Philippine Sea. The southward component of this circulation near the western boundary causes the NEC bifurcation latitude to shift northward. In addition to the local monsoonal wind forcing, equatorward propagating coastal Kelvin waves reflected by westward propagating Rossby waves generated at midlatitudes are also thought to alter the NEC bifurcation latitude [*Qu and Lukas*, 2003; *Chen and Wu*, 2011].

Because long-term data are limited, only a few studies have focused on year-to-year variation in the NEC bifurcation. *Qiu and Lukas* [1996] used a numerical model to show that the NEC bifurcation latitude shifts

poleward 1 year after an El Niño event and shifts equatorward during La Niña. They also suggested that NEC is controlled by basin-wide wind stress curl anomaly (WSCA). One year after El Niño, positive WSC intensifies and tends to shift northward the zero WSC line, affecting the NEC bifurcation. *Kim et al*. [2004] also found that meridional migration of NEC bifurcation is strongly influenced by El Niño-Southern Oscillation (ENSO). They argued that this variation can be attributed to westward propagation of upwelling (downwelling) Rossby waves generated by winds in the central equatorial Pacific and by an anomalous anticyclonic (cyclonic) WSC located in the western North Pacific when a warm (cold) event matures.

Recently, *Qiu and Chen* [2010] (*QC10*, hereafter) found that sea surface height anomaly (SSHA) in the domain of 12°N–14°N, 127°E–130°E off the Philippine coast could explain 92% of the variance of the NEC bifurcation latitude. They suggested that the bifurcation is largely determined by wind forcing in a band defined by 12°N–14°N and 140°E–170°E and that its low-frequency variability cannot be fully represented by the Niño-3.4 index. *Zhai and Hu* [2013] found that the Niño-3.4 index does not correlate well with the NEC transport either near the western boundary or at the date line, but only relates to the southern branch of the NEC transport along the Philippine coast. This result indicates that the NEC bifurcation variations do not correlate with the Niño-3.4 index very well due to the close relationship between the NEC bifurcation latitude and the NEC transport along the Philippine coast. Aside from ENSO, some other factors should be taken into account concerning this issue. *Zhai et al*. [2013] emphasized the NEC transport at 137°E correlated well with Pacific Decadal Oscillation (PDO) [*Trenberth and Hoar*, 1997; *Alley et al*., 2003] from 1975 to 2005. They associated the NEC transport change at 137°E with the decadal fluctuation of PDO, focusing after the year of 1974. Our work is aimed at identifying those factors that affect the NEC bifurcation variations on decadal time scales, and further quantifying their contributions during different time periods. By using surface wind data together with outputs from a well-validated numerical ocean model, we divide the time interval from 1961 to 2009 into three periods and investigate potential factors and/or mechanisms affecting the NEC bifurcation during each of the periods.

2. Model Description and Climate Indices

Forty-five year current velocity data from 1961 to 2005 used in this study are from the North Pacific Ocean (NPO) model [*Hsin et al*., 2008; *Hsin et al*., 2012] based on the Princeton Ocean Model (POM). On the basis of hydrostatic approximation, this model solves the three-dimensional primitive equations for the momentum, salt, and heat, and evaluates turbulence by the level 2.5 Mellor-Yamada scheme.

The NPO model covers the domain from 16°S to 60°N and 99°E to 77°W with a nonuniform resolution in the horizontal, 40 km at the equator and 20 km on the northern boundary. There are 26 sigma levels in the vertical. The model is driven by the monthly climatological wind stress reanalyzed by the National Centers for Environmental Prediction/National Center for Atmospheric Research (NCEP/NCAR). After spinning up from rest for 50 years, the model is subsequently forced by the NCEP/NCAR reanalysis version 1 wind data from 1948 to 1978 and version 2 wind data from 1979 to 2005. Monthly climatological sea surface temperature (SST) data derived from the NCEP/NCAR reanalysis are used as surface boundary condition during spin-up. The 6 h AVHRR SST (2.5° × 2.5°) from NCEP/NCAR is used for the period between 1948 and 1981. From 1982 to 2005, weekly SST data determined by optimal interpolation with a spatial resolution of 1° x 1° from the Data Support Section at the Computational and Information Systems Laboratory of NCAR (http://dss.ucar.edu/) are used. A detailed description of the NPO model has been given by *Hsin et al*. [2012]. Moreover, the modeled SSHA patterns, NEC bifurcation, and propagating Rossby wave signals corroborate with those inferred from the satellite altimeter measurements (figures not shown).

The PDO is a climate index (http://jisao.washington.edu/pdo/PDO.latest) based on the North Pacific SST variations [*Mantua et al*., 1997]. Warm (positive index) and cold (negative index) phases can persist for decades, although these decadal cycles have broken down recently [*Wu*, 2013, Figure 1a]. On the other hand, the Niño-3.4 index (http://www.cpc.ncep.noaa.gov/data/indices/sstoi.indices) is adopted from NOAA to represent the ENSO variability in this study.

3. Results

On both seasonal and interannual time scales, Rossby waves generated in the interior ocean are thought to be of vital importance for the migration of the NEC bifurcation latitude [*Qiu and Lukas*, 1996; *Qu and Lukas*,
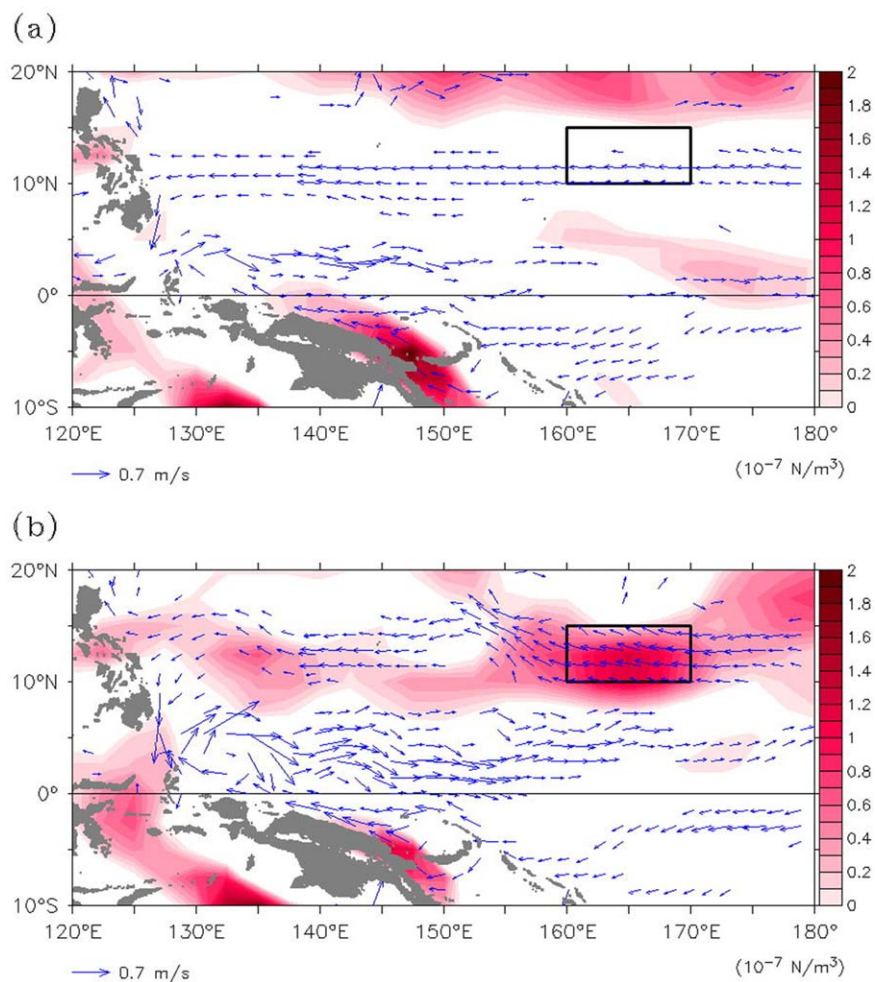
Figure 1. Wind stress curl anomalies generated from NCEP/NCAR (shading) together with modeled velocity field (vectors) where the magnitude larger than 0.2 m/s is presented. (averaged from 0 to 50 m) in (a) July 1984 and (b) July 2003. Vector scale is 0.7 m/s. The black rectangle identifies the region from 10–15°N and 160–170°E in the central equatorial Pacific. Contour interval for wind stress curl is 10^{-8} Nm^{-3}.

2003; *QC10*]. The upwelling (downwelling) Rossby waves induced by wind stress anomalies cause northward (southward) changes in the NEC bifurcation latitude [*Kim et al.*, 2004]. Figure 1 shows the WSCA and modeled circulation patterns in July 1984 versus July 2003 in the western Pacific. The black rectangle (10°N–15°N, 160°E–170°E; C-BOX hereafter) highlights the region where Rossby waves are effectively generated by WSCAs. Red shading indicates cyclonic WSCA that generates upwelling Rossby waves. For clarity, only velocities larger than 0.2 m/s are depicted. In July 1984, no clear positive WSCA occurred in C-BOX. At the same time, few Rossby waves were passing and the NEC flowed smoothly until bifurcating at approximately 10°N–12°N near the western boundary (Figure 1a). On the contrary, large positive WSCA around C-BOX in July 2003 generated upwelling Rossby waves and forced the NEC poleward until it ultimately bifurcated at about 12°N–16°N (Figure 1b). Similar patterns are seen in the altimeter-based SSHA data (figures not shown).

Rossby waves may not be the only factor causing the NEC bifurcation to migrate, but their presence seems crucial. Figure 2 shows the meridional velocity anomalies averaged from 10°N to 15°N. From 1982 to 1992, some weak Rossby wave signals propagate westward (e.g., March to December 1983 and March to September 1991), but they seem to be too weak to induce a significant shift in the NEC bifurcation (Figure 2a). From 1993 to 2005, more intense Rossby waves are generated at 170°E and propagate westward until they approach the western boundary (Figure 2b). In contrast to Figure 2a, the Rossby waves tend to strengthen as they move westward and attain their greatest strength near the western boundary in 1993–2005. Modeled meridional
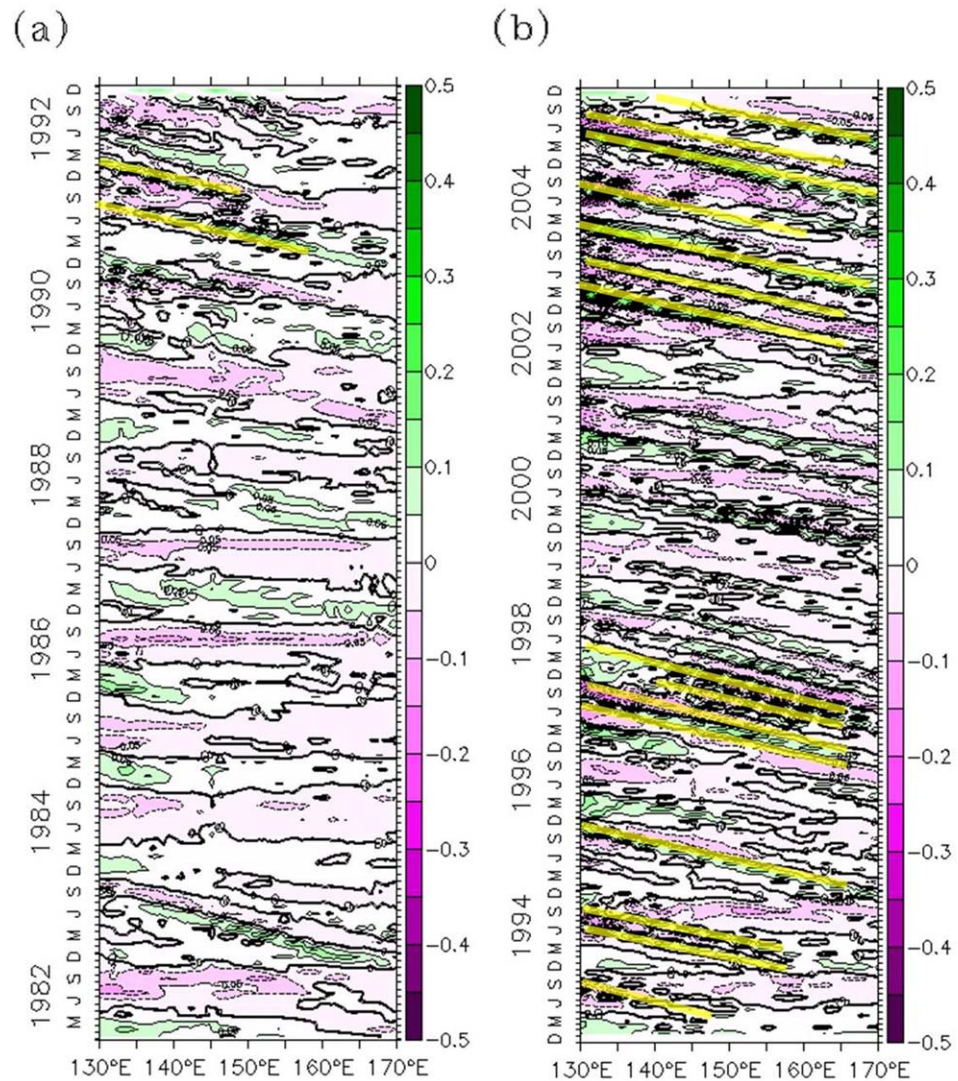
Figure 2. Meridional velocity anomalies in the region of 130–170°E (a) from 1982 to 1992 and (b) from 1993 to 2005. Data are averaged over the 10–15°N region. Contour interval is 0.05 m/s. Rossby waves are highlighted with yellow lines

velocity anomalies also demonstrate that this phenomenon is especially obvious during January 1994 to September 1995, September 1996 to January 1998, and January 2002 to December 2005 (Figure 2b). These periods correspond well with the time intervals during which the NEC bifurcated more northward investigated by *QC10* using the satellite altimeter SSH measurements (*Qiu and Chen*, 2010, Figure 2a).

Figure 3 shows the WSCA in C-BOX. From 1976 to 1992, C-BOX exhibits weakly negative WSCA, except around 1991–1992 (Figure 3a). However, from 1993 to 2009, a large positive WSCA appears in C-BOX, especially during 1996–1997 and 2002–2004 (Figure 3b). The wind pattern can be compared to the NPO simulated sea surface height pattern to identify the connections between these features. In other words, it is likely that the positive WSCA in C-BOX generates westward propagating upwelling Rossby waves which shift the NEC poleward and result in a higher bifurcation latitude of the NEC.

4. Mechanisms

According to Figure 2, Rossby waves were nearly absent prior to 1992 but prevailed after 1993. This raises the question of why Rossby waves do not prevail all the time. To investigate the main factors generating the Rossby waves, we divided the time interval of 1976–2009 into two periods: 1976–1992, and 1993–2009. The year 1976 marks one of the regime shifts of the PDO. Furthermore, both *Merrifield* [2011] and
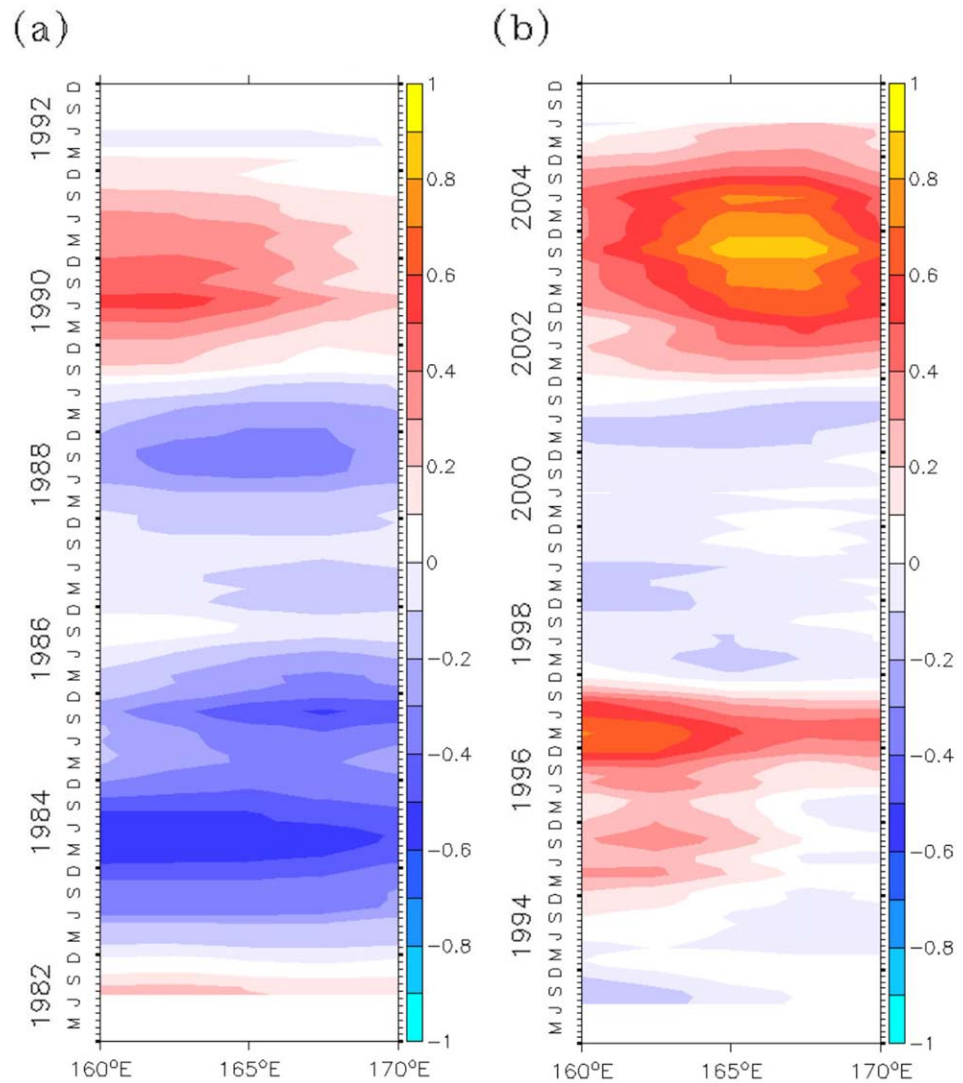
Figure 3. Wind stress curl anomalies in the region of 160–170°E (a) from 1982 to 1992 and (b) from 1993 to 2005. Data are averaged over the 10–15°N region. Contour interval for wind stress curl anomaly is 10^{-8} Nm^{-3}.

Qiu and Chen [2012] indicate that the early 1990s marked another shift in trend for the oceanic and atmospheric variables in the low-latitude western Pacific Ocean. *Merrifield* [2011] found that unlike the increasing trend of 10 mm yr^{-1} observed in 1993–2009, the sea level trend based on available tide gauges in the western tropical Pacific was nearly zero prior to 1992 (*Merrifield*, 2011, Figure 6). Relationships between NEC and ENSO have been mentioned in several studies [e.g., *Qiu and Joyce*, 1992; *Kashino et al.*, 2009], and connections between ENSO and PDO have also been discussed frequently [*Zhang et al.*, 1997; *Evans et al.*, 2001; *Wu* 2013]. Therefore, it is reasonable to investigate how PDO might affect the circulation pattern of the NEC and to analyze the effect of combined ENSO and PDO influences.

Figure 4a compares the WSCA time series averaged over the C-BOX with the Niño-3.4 and PDO indices in the first period, 1976–1992, and their correlation coefficients are listed in Table 1. The correlation between the WSCA and Niño-3.4 index reaches 0.62 and that between the WSCA and PDO index reaches −0.61. The opposing PDO and ENSO match each other in strength and neutralize their combined effects on the WSCA. This results in the WSCA in C-BOX to have little correlation to elsewhere in the North Pacific as shown in Figure 4b, which shows the correlation map between the WSCA in C-BOX and those in the North Pacific during 1976–1992. It seems that the negative-to-positive phase change of PDO has made the effects of ENSO on the WSCA weak in C-BOX (Figure 4b).
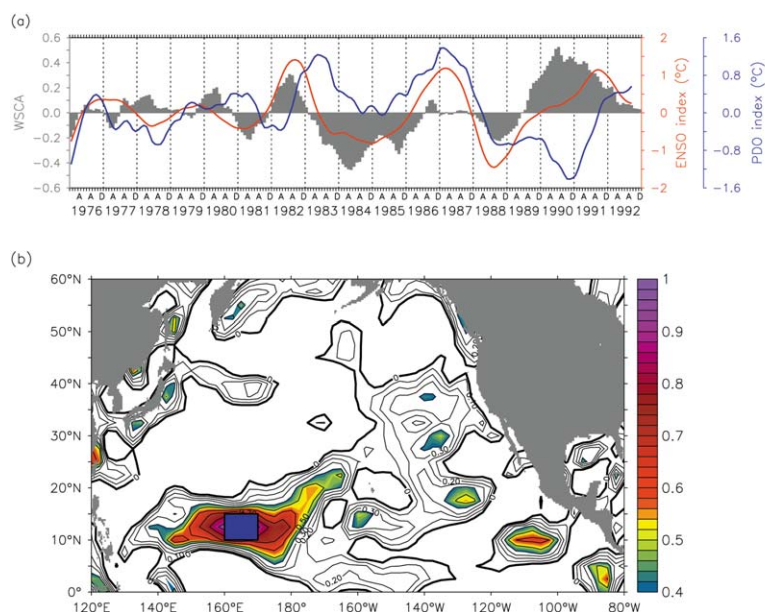
WANG ET AL.   6673

Figure 4. (a) Time series of wind stress curl anomaly averaged in the region of 10–15°N and 160–170°E (gray bars, units: 10^{-7} Nm^{-3}), together with Niño-3.4 (red curve, units: °C), PDO (blue curve, units: °C) and (b) the correlation coefficient between wind stress curl anomaly in the region of 10–15°N and 160–170°E and those in the North Pacific from 1976 to 1992. Correlation coefficients in that are larger than or equal to 0.4 are shown in colored shading and those larger than 0 but less than 0.4 are shown by contours. Contour interval is 0.1.

In the second period of 1993–2009, PDO replaces ENSO as a better match for the WSCA in C-BOX, with a correlation of 0.66 (Figure 5a). The PDO index is positive and reinforces its influences on the wind pattern in C-BOX. During the same interval, the correlation between the WSCA and Niño-3.4 index decreases to 0.48. Having both the positive correlations, PDO and ENSO impact the wind pattern in C-BOX constructively, amplifying the generation of Rossby waves during this period. The relative importance of PDO and ENSO can be quantified in terms of a linear regression model [*Newman et al.*, 2003] as

$$
\begin{pmatrix} W_1 \\ \vdots \\ W_n \end{pmatrix} = \begin{pmatrix} E_1 & P_1 \\ \vdots & \vdots \\ E_n & P_n \end{pmatrix} \begin{pmatrix} \alpha \\ \beta \end{pmatrix} + \begin{pmatrix} \varepsilon_1 \\ \vdots \\ \varepsilon_n \end{pmatrix}
$$

or

$$
W = \alpha \cdot E + \beta \cdot P + \varepsilon
$$

where W represents the WSCA in C-BOX, E is the Niño-3.4 index normalized by its variance, P is the PDO index also normalized by its variance, n is time (in years), and ε represents unexplained noise. The regression coefficients α and β of each period are listed in Table 1. From 1993 to 2009, we found that $\alpha = 0.04$ and $\beta = 0.51$, suggesting that the influence of PDO has nearly 13 times weight over that of ENSO. It is worth noting that the sum of α and β is only 0.55, implying that some other factors in addition to PDO and ENSO also play a role in generating Rossby waves in C-BOX.

Moreover, the correlation map of Figure 5b shows that the WSC pattern in the North Pacific best corresponds with that in C-BOX at two locations: 40°N, 160°W and 30°N, 145°W. The region of dominant PDO wind forcing is also located around 180°W–140°W, 35°N–50°N [see *Qiu*, 2003, Figure 2]. *Qiu* [2003] pointed out that the first EOF mode of the wind stress field lasting from 1982 to 2001 is centered at 40°N as found in the present study. The weighting function fits the PDO time series very well after 1992, while it is not significant from 1982 to 1991 [*Qiu*, 2003,

Table 1. Correlation and Linear Regression Coefficients

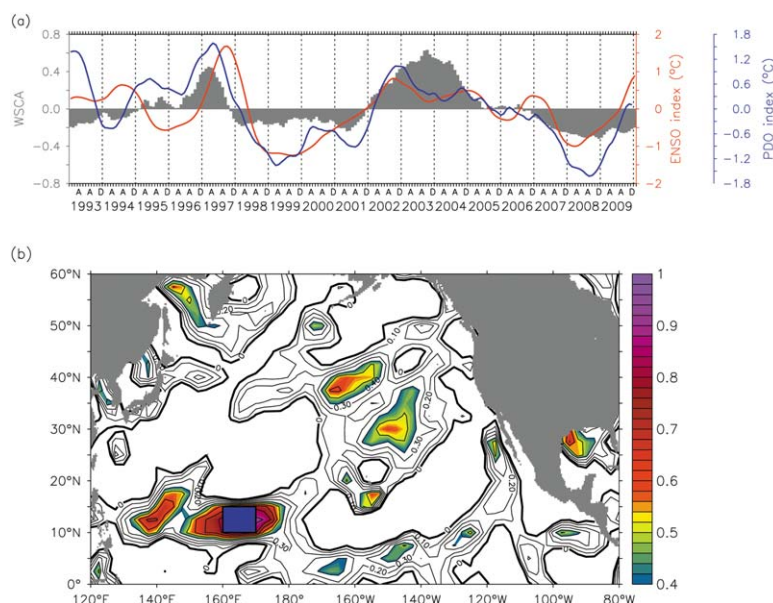|	Correlation WSCA-ENSO	Correlation WSCA-PDO	Linear Regression α	Linear Regression β
1961–1975	0.68	0.22	0.81	−0.32
1976–1992	0.62	−0.61	0.76	−0.73
1993–2009	0.48	0.66	0.04	0.51

Figure 5. Same as Figure 4 except from 1993 to 2009.

Figure 2]. Our correlation map, thus, supports the hypothesis that PDO dominated from 1993 to 2009 through connections between the WSC pattern in the midlatitudes and C-BOX. However, the most dominate mode of the North Pacific WSC pattern, according to *Qiu* [2003], explains only 17.8% of the total variance, implying that factors other than PDO contribute to the WSC variability. Future research is needed to further clarify the atmospheric processes responsible for this decadally varying, teleconnected wind stress pattern.

Figure 6 compares eddy kinetic energy (EKE) patterns between October 1985 and October 1997, which are chosen to represent the first and the second periods, respectively. The EKE is calculated based on the SSHA data from the NPO model simulation. The snapshot corresponds well with Figure 2 that the first period when few Rossby waves are generated and propagate westward, has less EKE, while the second period with more intense Rossby waves has more EKE in the western tropical North Pacific. Figure 7 displays the time series of WSCA averaged over the C-BOX and the EKE averaged in ($10°N–20°N$, $130°E–150°E$) from 1982 to 2005. The EKE prior to 1992 shows less variability compared to that afterward, and the correlation between the WSCA and EKE is only -0.05 during the first period, while it reaches 0.64 in the second period with the WSCA leading 7 months. Moreover, the EKE becomes larger responding to the large WSCA in C-BOX with a time lag of 7 months. This implies that the WSC pattern in C-BOX is independent of the EKE signals prior to 1992, but it becomes much more important for the Rossby wave generation and enhances the regional EKE level after 1993.
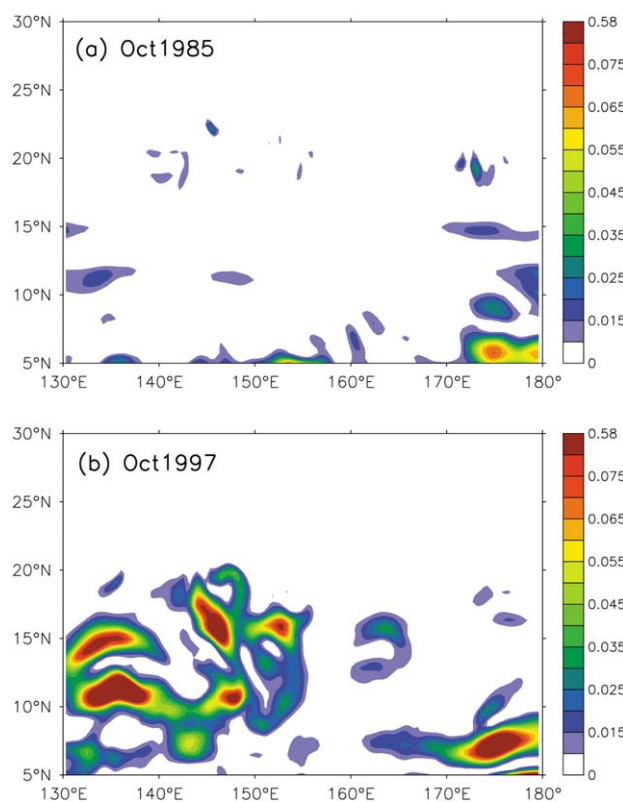
5. Discussion

Our analyses above have focused on the two contrasting periods following the 1976 regime shift in the Pacific Ocean. A relevant question to ask is how the WSCA in C-BOX is connected to ENSO and PDO prior to the 1976 regime shift when PDO was in its
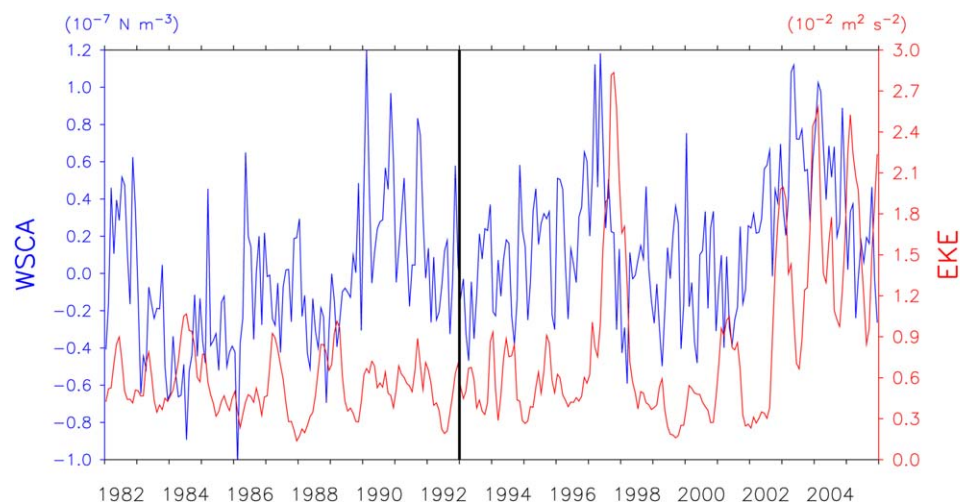

Figure 6. The EKE pattern in (a) October 1985 and (b) October 1997 (Units: m^2/s^2). Contour interval is 0.005.

Figure 7. Time series of wind stress curl anomalies (blue curve, units: Nm^{-3}) in C-BOX and the EKE (red curve, units: m^2/s^2) averaged in (10–20°N, 130–150°E) from 1982 to 2005.

negative phase. Earlier studies have always found a good correlation between ENSO and the interannual variability of the NEC bifurcation latitude [e.g., *Qiu and Lukas*, 1996; *Kim et al.*, 2004]. Does this imply ENSO exerts a stronger impact in the years before 1976, but less so recently? This turns out to be the case. *QC10* extended the time series of the NEC bifurcation latitude variability back in time to 1962 with the use of a dynamic model and proxy sea level anomalies. They found the interannual variability in the NEC bifurcation latitude is roughly correlated to the Niño-3.4 index (*Qiu and Chen*, 2010, Figure 7d). However, a closer inspection indicates that this consistence seems to break down during the recent years.

Figure 8a compares the WSCA averaged in C-BOX with the Niño-3.4 and PDO indices from 1961 to 1975. The wind data lead the Niño-3.4 index by 2 months with a correlation of 0.68, implying that the WSCA in C-BOX triggers Rossby waves during the developing phase of El Niños and that Rossby waves can propagate westward to affect the NEC bifurcation latitude at about the mature phase [*Qiu and Lukas*, 1996; *Kim et al.*, 2004]. In addition, the correlation between the PDO index and the WSCA is not significant (0.22) in 1961–1975. Utilizing the linear regression model described in section 4, we found that $\alpha=0.81$ and $\beta=-0.32$ for the 1961–1975 period, suggesting that ENSO dominates, but its weight is interfered by PDO. This indicates that the PDO-related WSCA during its negative phase is ineffective in generating Rossby waves in the central Pacific and affecting the NEC bifurcation latitude. As a result, ENSO dominates the NEC bifurcation variability before the 1976 regime shift.

Figure 8b shows the correlation between the WSCA in C-BOX and those in the North Pacific from 1961 to 1975. The map indicates that the wind pattern in C-BOX is coherent with that in the eastern equatorial Pacific at about 95°W–160°W and south of 10°N. This region is nearly collocated with the Niño-3.4 region (120°W–170°W, 5°N–5°S) but is closer to the eastern boundary. This is likely due to the fact that the along-equator WSCA was more zonally coherent from 1961 to 1975. During El Niño, there is a cyclonic and an anti-cyclonic WSC located on the two sides of the equator according to the Recharge Oscillator mechanism [*Jin*, 1997]. This map shows that the wind pattern in C-BOX corresponds with the positive WSCA in the northern tropical area during El Niño from 1961 to 1975. In addition, there seems to be a bridge-like band crossing from C-BOX to a midlatitude region (30°N–40°N, 120°W–135°W). This reveals that the wind pattern in C-BOX has some connections with that in the subtropical region near the eastern boundary.

This investigation demonstrates that the WSCA in C-BOX prior to the 1976 regime shift is largely associated with the wind field in the equatorial area, and is profoundly affected by ENSO. In contrast, the WSCA in C-BOX after 1992 is chiefly influenced by PDO when it is in its positive phase. The period in between (from 1976 to 1992) acts like a transition and the climate condition is gradually switching for PDO to take over the role of ENSO. It is this alternation of the dominant variability that controls the generation of Rossby waves in the 10°N–15°N band and affects the NEC bifurcation along the Philippine coast. This finding of ours is in agreement with *Zhai et al.* [2013] that PDO exerts a significant impact on the NEC variations after the regime shift.
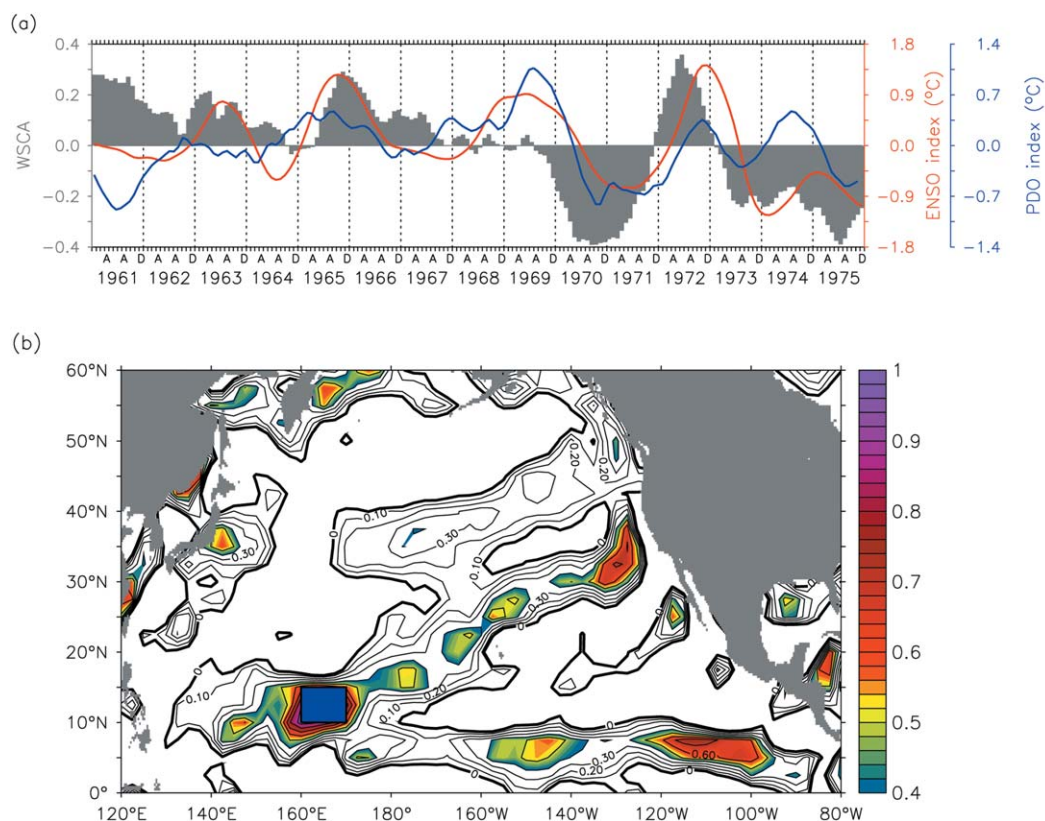
Figure 8. Same as Figure 4 except from 1961 to 1975.

From the first till the third period, there are two WSC anomaly areas with different signs and of nearly equal strength separated by 15°N. They are coincident with the two poles identified in *Chang and Oey* [2012], Figure 1b. The Philippines-Taiwan Oscillation (PTO) index is defined as the curl of the northern one minus the southern one, which might also imply only one of them is able to represent the significant pattern of this variability. Our C-BOX corresponds with their southern pole. Besides, C-BOX is located where cyclonic WSC anomaly is significant and enables to trigger Rossby waves to affect the NEC bifurcation. This work not only confirms the NEC bifurcation argument of *Chang and Oey* [2012], but further reveals the mechanism associated with the PDO and ENSO. For clarity, only significantly positive areas are displayed in the correlation maps (Figures 4b, 5b and 8b).

6. Concluding Remarks

Our model simulations show that the NEC bifurcates farther poleward when upwelling Rossby waves are intense. WSC anomalies in C-BOX are related closely to the excitation of Rossby waves and in turn control the NEC bifurcation fluctuations. We separated the time interval from 1976 to 2009 into two periods (1976–1992 and 1993–2009) to further investigate the factors generating Rossby waves. From 1976 to 1992,
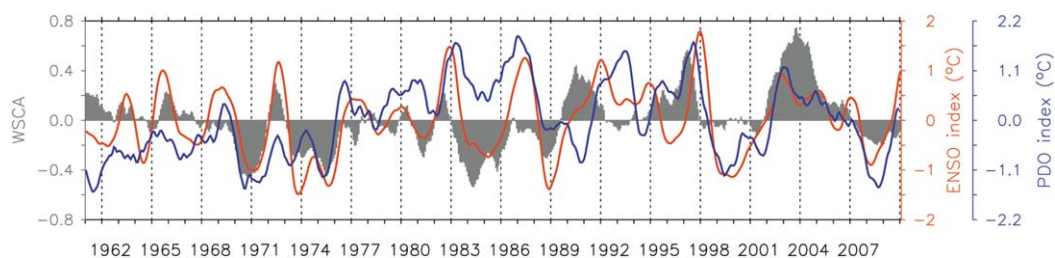

Figure 9. Time series of wind stress curl anomaly averaged in the region of 10–15°N and 160–170°E (gray bars, units: 10^{-7} Nm^{-3}), together with Niño-3.4 (red curve, units: °C), PDO (blue curve, units: °C) from 1961 to 2009.

following a regime shift to the positive PDO phase, PDO and ENSO match each other in strength and resulted in a neutralized effect on the WSCA in C-BOX. From 1993 to 2009, the strength of the canonical El Niño becomes weaker because the central-Pacific El Niño [*Kao and Yu*, 2009] tends to dominate in recent decades [*Yeh et al.*, 2009]. The central-Pacific El Niños are characterized by decreasing strength and increasing frequency particularly during the period after 1990 [*Yu et al.*, 2012]. On the other hand, the PDO index generally remains positive and strengthens its influences on the wind pattern. The PDO forcing consequently takes over the role of ENSO and dominates the WSCA variations in C-BOX.

Via a linear regression model, we show that the influence of PDO has nearly 13 times weight over that of ENSO during 1993–2009. This explains why the variation in the NEC bifurcation latitude in this period does not correspond well to ENSO as mentioned by *QC10*. Furthermore, the correlation map shows that the WSC pattern in the North Pacific corresponds best with that in C-BOX at two locations: 40°N, 160°W and 30°N, 145°W. The former location happens to be the region where PDO dominates. This further supports the hypothesis that the PDO forcing dominated the period from 1993 to 2009.

Prior to the 1976 regime shift in the negative PDO phase, the correlation map indicates that the wind pattern in C-BOX is correlated with the Niño-3.4 region. From 1961 to 1975, the wind data in C-BOX lead the Niño-3.4 index by 2 months with a correlation of 0.68, implying the WSCA in C-BOX triggers Rossby waves during the developing phase of El Niño. The westward propagating Rossby waves lead to a northerly NEC bifurcation at about the mature phase of El Niño. On the other hand, the correlation between the PDO index and the WSCA is not significant during this period, suggesting that the negative PDO phase fails to generate Rossby waves. The ENSO influence, hence, dominates during the period from 1961 to 1975.

Throughout the entire period (Figure 9), the correlation between ENSO and the wind pattern keeps decreasing from 1961 and nearly falls below the significance level in the last period. We emphasize that it is not appropriate to consider the wind pattern in C-BOX in the same frame for all years. Rossby waves are preferentially generated in either the negative PDO phase when the ENSO forcing dominates (such as during 1961–1976), or in the positive PDO phase when the ENSO signal is overshadowed (such as in 1993–2009). During the period when the positive PDO forcing tends to mitigate the ENSO signal, the resultant wind forcing is not strong enough to trigger the Rossby waves.

References

Alley, R. B., et al. (2003), Abrupt climate change, *Science*, *299*, 2005–2010, doi:10.1126/science.1081056.

Chang, Y.-L., and L. Y. Oey (2012), The Philippines-Taiwan Oscillation: Monsoon-like interannual oscillation of the subtropical-tropical western North Pacific Wind System and its impact on the ocean, *J. Clim.*, *25*, 1597–1618.

Chen, Z., and L. Wu (2011), Dynamics of the seasonal variation of the North Equatorial Current bifurcation, *J. Geophys. Res.*, *116*, C02018, doi:10.1029/2010JC006664.

Evans, M. N., M. A. Cane, D. P. Schrag, A. Kaplan, B. K. Linsley, R. Villalba, and G. M. Welington (2001), Support for tropically driven Pacific decadal variability based on paleoproxy evidence, *Geophys. Res. Lett.*, *28*, 3689–3692.

Hsin, Y.-C., C.-R. Wu, and P.-T. Shaw (2008), Spatial and Temporal Variations of the Kuroshio East of Taiwan, 1982–2005: A numerical study, *J. Geophys. Res.*, *113*, C04002, doi:10.1029/2007JC004485.

Hsin, Y.-C., C.-R. Wu, and S.-Y. Chao (2012), An updated examination of the Luzon Strait transport, *J. Geophys. Res.*, *117*, C03022, doi: 10.1029/2011JC007714.

Jin, F. F. (1997), An equatorial ocean recharge paradigm for ENSO. Part I: Conceptual model, *J. Atmos. Sci. 54*, 811–829.

Kao, H.-Y., and J.-Y. Yu (2009), Contrasting eastern-Pacific and central-Pacific types of El Niño, *J. Clim.*, *22*, 615–632, doi:10.1175/2008JCLI2309.1.

Kashino, Y., N. Espana, F. Syamsudin, K. J. Richards, T. Jensen, P. Dutrieux, and A. Ishida (2009), Observations of the North Equatorial Current, Mindanao Current, and the Kuroshio Current system during the 2006/07 El Niño and 2007/08 La Niña, *J. Oceanogr.*, *65*, 325–333.

Kim, Y. Y., T. Qu, T. Jensen, T. Miyama, H. Mitsudera, H.-W. Kang, and A. Ishida (2004), Seasonal and interannual variations of the North Equatorial Current bifurcation in a high-resolution OGCM, *J. Geophys. Res.*, *109*, C03040, doi:10.1029/2003JC002013.

Lukas, R., E. Firing, P. Hacker, P. L. Richardson, C. A. Collins, R. Fine, and R. Gammon (1991), Observations of the Mindanao Current during the Western Equatorial Pacific Ocean Circulation Study, *J. Geophys. Res.*, *96*, 7089–7104.

Mantua, N. J., S. R. Hare, Y. Zhang, J. M. Wallace, and R. C. Francis (1997), A Pacific interdecadal climate oscillation with impacts on salmon production, *Bull. Am. Meteorol. Soc.*, *78*(6), 1069–1079.

Merrifield, M. A. (2011), A shift in western tropical Pacific sea level trends during the 1990s, *J. Clim.*, *24*, 4126–4138.

Newman, M., G. P. Compo, and M. A. Alexander (2003), ENSO-forced variability of the Pacific Decadal Oscillation, *J. Clim.*, *16*, 3853–3857.

Qiu, B. (2003), Kuroshio Extension variability and forcing of the Pacific decadal oscillations: Responses and potential feedback, *J. Phys. Oceanogr.*, *33*, 2465–2482.

Qiu, B., and S. Chen (2010), Interannual-to-decadal variability in the bifurcation of the North Equatorial Current off the Philippines, *J. Phys. Oceanogr.*, *40*, 2525–2538, doi:10.1175/2010JPO4462.1.

Qiu, B., and S. Chen (2012), Multi-decadal sea level and gyre circulation variability in the northwestern tropical Pacific Ocean, *J. Phys. Oceanogr.*, *42*, 193–206, doi:10.1175/JPO-D-11-061.1.

Qiu, B., and T.M. Joyce (1992), Interannual variability in the mid- and low-latitude western North Pacific, *Phys. Oceanogr.*, *22*, 1062–1079.

Qiu, B., and R. Lukas (1996), Seasonal and interannual variability of the North Equatorial Current, the Mindanao Current and the Kroshio along the Pacific western boundary, *J. Geophys. Res.*, *101*, 12,315–12,330.

Qu, T., and R. Lukas (2003), The bifurcation of the North Equatorial Current in the Pacific, *J. Phys. Oceanogr.*, *33*, 5–18.

Trenberth, K. E., and T. J. Hoar (1997), El Niño and climate change, *Geophys. Res. Lett.*, *24*, 3057–3060.

Wu, C.-R. (2013), Interannual modulation of the Pacific Decadal Oscillation (PDO) on the low-latitude western North Pacific, *Prog. Oceanogr.*, *110*, 49–58, doi:10.1016/j.pocean.2012.12.001.

Yeh, S.-W., J.-S. Kug, B. Dewitte, M.-H. Kwon, B. P. Kirtman, and F.-F. Jin (2009), El Niño in a changing climate, *Nature*, *461*, 511–514, doi: 10.1038/nature08316.

Yu, J.-Y., M.-M. Lu, and S.-T. Kim (2012), A change in the relationship between tropical central Pacific SST variability and the extratropical atmosphere around 1990, *Environ. Res. Lett.*, *7*, 034025, doi:10.1088/1748-9326/7/3/034025.

Zhai, F., and D. Hu (2013), Revisit the interannual variability of the North Equatorial Current transport with ECMWF ORA-S3: Interannual variability of NEC transport, *J. Geophys. Res. Oceans*, *118*, 1349–1366, doi:10.1002/jgrc.20093.

Zhai, F., D. Hu, and T. Qu (2013), Decadal variations of the North Equatorial Current in the Pacific at 137°E, *J. Geophys. Res. Oceans*, *118*, 4989–5006, doi:10.1002/jgrc.20391.

Zhang, Y., J. M. Wallace, and D. S. Battisti (1997), ENSO-like interdecadal variability: 1900–93, *J. Clim.*, *10*, 1004–1020.